

# mROS-calcium feedback loop promotes lethal ventricular arrhythmias and sudden cardiac death in early myocardial ischemia

DANYA ZHOU<sup>1,2\*</sup>, YE ZHANG<sup>1\*</sup>, MENGTING ZHU<sup>1\*</sup>, XIAOJUN ZHANG<sup>3</sup>, XIAOJUAN ZHANG<sup>1</sup>, JUNYAO LV<sup>1</sup>, WANTING TANG<sup>1</sup>, QI WENG<sup>1</sup>, YANG LIN<sup>1</sup>, LEJUN TONG<sup>1</sup>, ZHIWEI ZHONG<sup>1</sup>, YANMEI ZHANG<sup>4</sup>, MENGXUAN ZHANG<sup>1</sup>, MINCHAO LAI<sup>5</sup> and DIAN WANG<sup>1</sup>

<sup>1</sup>Department of Forensic Medicine, Shantou University Medical College, Shantou, Guangdong 515041;

<sup>2</sup>School of Forensic Medicine, Xinxiang Key Laboratory of Forensic Toxicology, Xinxiang Medical University, Xinxiang,

Henan 453003; <sup>3</sup>Institute of Marine Sciences and Guangdong Provincial Key Laboratory of Marine Biotechnology, Shantou University, Shantou, Guangdong 515041; <sup>4</sup>Department of Pharmacology, Shantou University Medical College;

<sup>5</sup>Department of Neurology, First Affiliated Hospital of Shantou University Medical College, Shantou, Guangdong 515041, P.R. China

Received August 2, 2023; Accepted October 23, 2023

DOI: 10.3892/ijmm.2023.5329

**Abstract.** Lethal ventricular arrhythmia-sudden cardiac death (LVA-SCD) occurs frequently during the early stage of myocardial ischemia (MI). However, the mechanism underlying higher LVA-SCD incidence is still poorly understood. The present study aimed to explore the role of mitochondrial reactive oxygen species (mROS) and Ca<sup>2+</sup> crosstalk in promoting LVA-SCD in early MI. RyR2 S2814A mice and their wild-type littermates were used. MitoTEMPO was applied to scavenge mitochondrial ROS (mROS). Mice were subjected to severe MI and the occurrence of LVA-SCD was evaluated. Levels of mitochondrial ROS and calcium (mitoCa<sup>2+</sup>), cytosolic ROS (cytoROS), and calcium (cytoCa<sup>2+</sup>), RyR2 Ser-2814

phosphorylation, CaMKII Met-282 oxidation, mitochondrial membrane potential (MMP), and glutathione/oxidized glutathione (GSH/GSSG) ratio in the myocardia were detected. Dynamic changes in mROS after hypoxia were investigated using H9c2 cells. Moreover, the myocardial phosphoproteome was analyzed to explore the related mechanisms facilitating mROS-Ca<sup>2+</sup> crosstalk and LVA-SCD. There was a high incidence (~33.9%) of LVA-SCD in early MI. Mice who underwent SCD displayed notably elevated levels of myocardial ROS and mROS, and the latter was validated in H9c2 cells. These mice also demonstrated overloads of cytoplasmic and mitochondrial Ca<sup>2+</sup>, decreased MMP and reduced GSH/GSSG ratio, upregulated RyR2-S2814 phosphorylation and CaMKII-M282 oxidation and transient hyperphosphorylation of mitochondrial proteomes in the myocardium. mROS-specific scavenging by a mitochondria-targeted antioxidant agent (MitoTEMPO) corrected these SCD-induced alterations. S2814A mice with a genetically inactivated CaMKII phosphorylation site in RyR2 exhibited decreased overloads in cytoplasmic and mitochondrial Ca<sup>2+</sup> and demonstrated similar effects as MitoTEMPO to correct SCD-induced changes and prevent SCD post-MI. The data confirmed crosstalk between mROS and Ca<sup>2+</sup> in promoting LVA-SCD. Therefore, we provided evidence that there is a higher incidence of LVA-SCD in early MI, which may be attributed to a positive feedback loop between mROS and Ca<sup>2+</sup> imbalance.

*Correspondence to:* Professor Dian Wang, Department of Forensic Medicine, Shantou University Medical College, 22 Xinling Road, Shantou, Guangdong 515041, P.R. China  
E-mail: g\_dwang@stu.edu.cn

\*Contributed equally

**Abbreviations:** CAL, coronary artery ligation; ETC, electron transport chain; KEGG, Kyoto Encyclopedia of Genes and Genomes; LVA, lethal ventricular arrhythmia; MAM, mitochondria-associated sarcoplasmic reticulum membrane; MI, myocardial ischemia; mROS, mitochondrial reactive oxygen species; MMP, mitochondrial membrane potential; ox-CaMKII, oxidized Ca<sup>2+</sup>/calmodulin-dependent protein kinase; RIRR, ROS-induced ROS release; RyR2, ryanodine receptor 2; SCD, sudden cardiac death; TCA, tricarboxylic acid cycle

**Key words:** lethal ventricular arrhythmia, sudden cardiac death, early myocardial ischemia, mROS-Ca<sup>2+</sup> loop, phosphoproteome

## Introduction

Myocardial ischemia (MI) is the leading cause of death globally, accounting for ~16% of total deaths (1). Nearly half of MI cases die as a result of sudden cardiac death (SCD) and lethal ventricular arrhythmia (LVA) is the most common cause of SCD (2). Although progress has been made in supportive care, efforts to prevent MI-induced SCD have failed; cases are

increasing and becoming a major public health problem worldwide (3). Clinically, SCD induced by MI commonly occurs within the first hour after a heart attack and the incidence decreases exponentially thereafter (4,5). Therefore, the early period is the most dangerous period for LVA-SCD and is a key time to prevent SCD. Nevertheless, the underlying mechanism of LVA-SCD during this period is not fully understood.

As the primary source of reactive oxygen species (ROS) during MI, mitochondrial (m)ROS predispose individuals to LVA (6). Studies have uncovered crosstalk between mROS and  $\text{Ca}^{2+}$  signaling via the mitochondria-associated sarcoplasmic reticulum membrane (MAM) (7,8).  $\text{Ca}^{2+}$ /calmodulin-dependent protein kinases (CaMKs), which are localized within the MAM, are activated upon oxidation at methionine 282 (9). In turn, oxidized (ox-)CaMKII phosphorylates ryanodine receptor 2 (RyR2) at serine 2814 via the MAM, leading to diastolic  $\text{Ca}^{2+}$  leak from the sarcoplasmic reticulum and triggering malignant arrhythmia (10). CaMKII-M282 oxidation and RyR2-S2814 phosphorylation are increased in patients with atrial fibrillation and ventricular tachycardia (11,12), suggesting that both the mROS and relevant  $\text{Ca}^{2+}$  leak can lead to LVA. To the best of our knowledge, however, it has not been determined whether mROS- $\text{Ca}^{2+}$  crosstalk serves a pivotal role in the development of LVA-SCD in early MI. The present study aimed to explore the underlying mechanism of LVA-SCD within the early stage of MI (up to 30 min post-MI), focusing on the mROS- $\text{Ca}^{2+}$  crosstalk.

## Materials and methods

**Experimental mice.** The present study was approved by the Medical Animal Care and Welfare Committee at Shantou University Medical College (Shantou, China; approval no. SUMC2020-035). Animal studies were performed according to the guidelines from the National Institutes of Health (NIH) Guide for the Care and Use of Laboratory Animals (13).

A point mutation of serine (S) to alanine (A) at position 2814 of the RyR2 (hereafter referred to as 'S2814A') was introduced in C57/BL6 mice using CRISPR/Cas gene-editing technology (Data S1) by Cyagen Biosciences to address the role of RyR2-S2814 phosphorylation in  $\text{Ca}^{2+}$  balance. They were bred and their offspring were raised, mated, and bred at the Laboratory Animals Center of Shantou University Medical College (Shantou, China) under 22–24°C, 60–65% humidity and a 12/12-h light/dark cycle. Since males are more likely to have coronary artery disease than females (14), the present study used only male offspring of the fourth to five generation (n=32, age, ~8 weeks, 25–30 g). Animals had free access to rodent chow and clean drinking water. Specific pathogen-free grade C57/BL6 male mice (n=130, age, ~8 weeks, 25–30 g) were obtained from Charles River Laboratories (Beijing, China), and they were kept in the same housing conditions.

**Acute MI mouse model and MitoTEMPO treatment.** S2814A homozygous mutant (confirmed by DNA sequencing; Supplementary Materials and methods) male mice and their wild-type male littermates (n=152, age, ~8 weeks, 25–30 g) were subjected to left coronary artery ligation (CAL). Briefly, mice were anesthetized using 30 mg/kg body weight 1% pentobarbital

sodium in saline (Sigma-Aldrich; Merck KGaA) through intraperitoneal injection. Then, lead II electrocardiogram (ECG) was monitored using BL-420 Biological-Functional Experimental System (Chengdu Taimeng Co., Ltd.). When the animal was deeply anesthetized (no response to pinching of the toes or fingers), artificial ventilation was established with a tidal volume of 2 ml/kg, an inspiratory/expiratory ratio of 1:2 and a respiratory rate of 115 breaths/min. The thoracic cavity was opened, the pericardium was cut and the main left coronary artery was ligated. Following CAL, the elevated T waves indicated the success of the ligation. Some mice developed LVA-SCD (MI-SCD group, n=21). The remaining mice, who maintained a relatively normal ECG and survived  $\geq 70$  min after CAL, were defined as stable group (MI-S group, n=41). S2814A mice were similarly subjected to MI, which was defined as transgenic group (TG-MI group, n=32). To characterize the protective mechanism of the point mutation, only mice that survived early MI were used for experiments.

A group of wild-type mice (n=26) were administered MitoTEMPO (2.0 mg/kg in saline; Sigma-Aldrich; Merck KGaA; cat. no. SML0737) via tail vein injection 15 min before CAL operation, which as defined as the MT-MI group, and we only recruited the surviving mice (n=21) to determine the specific protective mechanism of MitoTEMPO. Sham-operated mice (SO group, n=32) were anesthetized and subjected to thoracotomy as aforementioned, excluding those with abnormal ECG after operation. Surviving mice were euthanized by over-anesthesia with sodium pentobarbital (90 mg/kg) (15). Mice who experienced massive hemorrhage during the operation were excluded. Left ventricles were immediately harvested after death and stored at -80°C for further experiments.

**ECG analysis.** The corrected QT interval (QTc) was calculated with Bazett's formula ( $\text{QTc} = \text{QT interval} / \sqrt{\text{RR interval}}$ ) and RRI was normalized by heart rates (16). For T wave variation analysis, one typical case was selected from each experimental group and 10 complete ECG data (P wave, QRS complex, and T wave) were read every 5 min for the first 20 min after MI. Amplitudes of T waves were collected every 8 msec and integrated to produce a polyline chart to determine T wave variation (17).

**Hypoxic model of H9c2 and dynamic detection of mROS.** A hypoxia model of H9c2 cells (purchased from the Cell Bank of Chinese Academy of Sciences, Shanghai, China) was generated to explore changes in mROS after hypoxia. H9c2 cells were inoculated into 3.5-cm dishes (total cells:  $3 \times 10^5$ ) and grown (37°C, 5%  $\text{CO}_2$ ) to 60–80% confluence in high-glucose DMEM (Gibco) supplemented with 10% fetal bovine serum. Penicillin/streptomycin (100 U/100  $\mu\text{g}/\text{ml}$ ) was used. The cells were incubated at 37°C in Baker Ruskinin's InvivO<sub>2</sub> (400) hypoxia workstation (I&L Biosystems GmbH) in 1%  $\text{O}_2$ , 5%  $\text{CO}_2$  and 94%  $\text{N}_2$  for 15, 30, 45 or 70 min, respectively. A group of cells undergoing 15 min hypoxia was also pretreated with MitoTEMPO (0.5  $\mu\text{M}$ ) at 37°C for 30 min. Cells were incubated at 37°C with MitoSOX™ probe (Thermo Fisher Scientific, Inc.; 5  $\mu\text{M}$ ) for 15 min, and fluorescence images (x200 magnification) were obtained in a Carl Zeiss LSM 880 confocal microscope (Carl Zeiss GmbH) to evaluate

mROS levels. The excitation wavelength ( $\lambda_{Ex}$ ) and emission wavelength ( $\lambda_{Em}$ ) were set according to the manufacturer's instructions. The fluorescence intensity was quantified using Image J software (Image J 1.52i; NIH).

**Detection of ROS and  $Ca^{2+}$  in cytoplasm and mitochondria.** ROS and  $Ca^{2+}$  were directly measured by relative fluorescent probes. Briefly, hearts were immediately retrieved after mouse death and pre-cooled in a frozen sectioning machine for 20 min. Then, myocardial cryosections ( $5 \mu\text{M}$ ) were prepared immediately, followed by incubation at  $37^\circ\text{C}$  with dihydroethidium (DHE;  $2 \mu\text{M}$ ; 30 min), MitoSOX ( $5 \mu\text{M}$ ; 15 min), Fura-2 AM ( $1 \mu\text{M}$ ; 30 min; all Thermo Scientific) or Rhod-2 AM ( $2 \mu\text{M}$ ; 15 min; MedChemExpress) to detect levels of ROS and  $Ca^{2+}$  in the cytoplasm and mitochondria, respectively. DAPI ( $50 \mu\text{l}$ , Beyotime) staining (10 min at room temperature) was used to visualize nuclei of cardiomyocytes. Fluorescence (x200 magnification) was measured using a Carl Zeiss LSM 800 confocal microscope (Carl Zeiss) and the excitation wavelength was set according to the manufacturer's instructions. The fluorescence intensity was quantified using Image J software.

**Measurement of mitochondrial membrane potential (MMP).** MMP was assessed by JC-1 staining according to manufacturer's instructions. First, myocardial mitochondria from the myocardium of the experimental mice were isolated with Tissue Mitochondria Isolation kit (Beyotime Institute of Biotechnology). MMP ( $\Delta\Psi\text{m}$ ) assay kit (Beyotime Institute of Biotechnology) with the JC-1 probe was used to detect MMP. Fluorescence images (x100 magnification) were obtained with an Olympus fluorescence microscope to detect JC-1 monomers (green fluorescence, low potential) and aggregates (red fluorescence, high potential) were detected. The fluorescence intensity was quantified using Image J software.

**Measurement of reduced glutathione/oxidized glutathione (GSH/GSSG) ratio.** Oxidized and total glutathione levels in the left ventricular tissue were measured with GSH and GSSG Assay kit (Beyotime), according to the manufacturer's protocols. GSH levels were calculated as follows:  $\text{GSH} = (\text{total glutathione} - \text{GSSG}) \times 2$ . Data are presented as the ratio of GSH to GSSG.

**Western blot assay.** The protein samples from ventricular tissue were separated by T-PER™ (Thermo Fisher Scientific) and concentration was measured by the bicinchoninic acid (BCA) assay kit (Beyotime). Next, an equal amount of protein ( $25 \mu\text{g}/\text{well}$ ) from each sample was separated by SDS-polyacrylamide gels (10%) and transferred to a PVDF membrane. After blocking with 2% BSA (Sigma-Aldrich, 1 h at room temperature) the membrane was incubated overnight at  $4^\circ\text{C}$  with primary antibodies against anti-ox-CaMKII (1:1,000, Millipore Sigma; cat. no. 07-1387), anti-CaMKII (1:000, Abcam; cat. no. ab181052), anti-phosphorylated (p-) RyR2S-2814 (1:500, Badrilla; cat. no. A010-31AP), anti-RyR2 (1:1,000, Thermo Fisher Scientific, Inc.; cat. no. C3-33) and anti-GAPDH (1:10,000, Abcam; cat. no. ab181602), respectively. Then the membranes were incubated with corresponding secondary antibodies horseradish peroxidase-linked anti-rabbit

Ig G (1:10,000, Abcam; cat. no. ab6721) or anti-mouse IgG (1:5,000, Abcam; cat. no. ab205719) for one hour at room temperature. Immunoblotting was imaged with a ChemiDoc MP (Bio-Rad Laboratories, Inc.) with ECL Western Blotting Substrate (Solarbio), and the blot densitometry was quantified using the Image Lab™ (v3.0) software (Bio-Rad). Expression of CaMKII-M282 oxidation and RyR2-S2814 phosphorylation was normalized to total levels of their respective proteins.

**Phosphoproteome analysis.** The phosphoproteome was analyzed according to previous studies (18,19). A total of 1 mg protein from each left ventricular myocardium was treated with the filter-aided sample preparation (FASP) method (18), followed by digestion with trypsin (1:50, w/w; Promega Corporation) overnight at  $37^\circ\text{C}$ . The peptides were then dried by vacuum centrifugation (1,000 g,  $-25^\circ\text{C}$ , 3 h), followed by phosphorylated peptide enrichment using the High-Select™  $\text{TiO}_2$  Phosphopeptide Enrichment kit (Thermo Fisher Scientific, Inc.), according to the manufacturer's instructions.

Tandem Mass Tag (TMT) six plex™ Label Reagent Set (Thermo Fisher Scientific, Inc.) was used to label the peptides. The mixture was subsequently desalted, concentrated, dried and lyophilized using a desalting column (C18 Stage Tips, Thermo). To increase phosphopeptide, fractionation of labeled peptides using Pierce™ High pH Reversed-Phase Peptide Fractionation kit (Thermo Fisher Scientific, Inc.) was performed before LC-tandem mass spectrometry (LC-MS/MS) analysis. Acquisition was performed on a Thermo Scientific™ Orbitrap Elite mass spectrometer (Thermo Fisher Scientific, Inc.), coupled to an EASY-nLC™ 1000 nano flow liquid chromatography (Thermo Fisher Scientific, Inc.) equipped with a  $75 \mu\text{m} \times 105 \text{ mm}$  PicoCHIP nano spray column packed with Reprosil-PUR C18-AQ,  $3 \mu\text{m}$ ,  $120 \text{ \AA}$  (New Objective, Inc.). A total of  $2 \mu\text{g}$  desalted peptide from each fraction were loaded onto PicoCHIP analytical column (New Objective) and the peptides were separated using a 120-min elution gradient at 300 nl/min [5-9% mobile phase B (acetonitrile, 0.1% formic acid) for 2 min, 9-27% for 90 min, 27-40% for 13 min, 40-90% for 5 min and 90-100% mobile phase B for 10 min]. Three replicates were performed for each group.

Electron Spray Ionization (ESI) voltage was set to 2.0 kV, capillary temperature was  $280^\circ\text{C}$ , nebuliser pressure (psi) was set to 100-300 bar, and cation mode was selected for acquisition. MS data (scan range 350-1,800 m/z) were acquired from Fourier transform mass spectrometry (FTMS) with a resolution of 60,000 at 200 m/z. Automatic gain control target was set to  $3 \times 10^6$ , and maximum injection time was 200 msec. MS2 data were acquired in FTMS mode with a resolution of 15,000 at 200 m/z. The 15 strongest ions with charges 2-5 were continuously separated in data dependent acquisition (DDA) mode for high-energy collision-induced dissociation at 40% normalized collision energy with a dynamic exclusion time set to 60 sec, excluding ions with single and unidentified charge states. All measurements were internally calibrated using the mass option. The data were analyzed (Data S1) using MaxQuant software (Max-Planck-Institute of Biochemistry, version 2.1.4.0, maxquant.org/) (20) and MSstats R package (version 2.2.7) to perform quality inspection and statistical analysis (21).

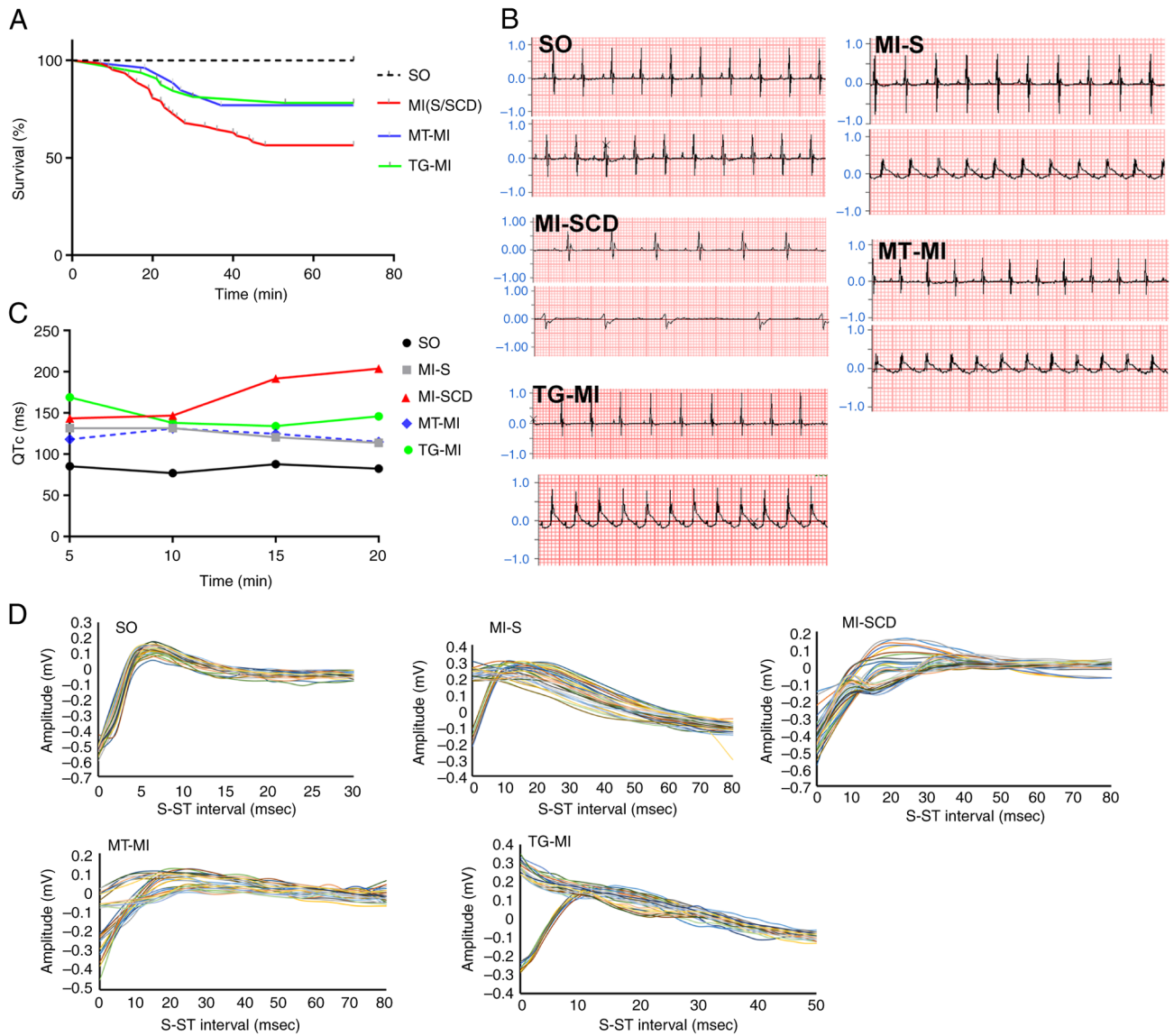


Figure 1. High incidence of LVA-SCD in early MI is prevented by MitoTEMPO treatment or S2814A mutation. (A) Kaplan-Meier curve (number of SCD cases to that of total cases: SO=0/32, MI-S/SCD=21/62, MT-MI=4/26, TG-MI=5/32), illustrating a high incidence of LVA-SCD in early MI and MitoTEMPO and S2814A mutation could reduce propensity for LVA-SCD. (B) Lead II ECG. Upper and lower traces show the ECGs before and after MI, respectively. (C) QTc. (D) T wave variability. LVA, lethal ventricular arrhythmia; SCD, sudden cardiac death; MI, myocardial ischemia; SO, sham operation; MT, MitoTEMPO; TG, transgenic; ECG, electrocardiogram; QTc, corrected QT.

According to the criteria of  $P < 0.05$ , fold-change (FC)  $> 1.2$  for up- and  $< 0.83$  for downregulation, the differentially expressed phosphorylated proteins (DEPPs) were screened. Functional enrichment analysis was performed using Metascape (<https://metascape.org/>, v3.5.20230501) and the Database for Annotation, Visualization and Integrated Discovery (DAVID, <https://david.ncifcrf.gov/>, Dec 2021) to determine enriched Kyoto Encyclopedia of Genes and Genomes (KEGG, <https://www.genome.jp/kegg/>, Nov 2022) pathways, Gene ontology (GO, [geneontology.org/](https://geneontology.org/)), biological process (BP), cellular component (CC) and molecular function (MF) (22).

**Statistical analysis.** Data were analyzed by SPSS (IBM Corp.; version 24.0) and are expressed as the mean  $\pm$  SD. Data were analyzed using one-way ANOVA followed by Dunnett's multiple comparisons post hoc test. Survival was assessed

by Kaplan-Meier curves and log-rank test. Figures were constructed using GraphPad Prism (version 8.0; GraphPad Software Inc.; Dotmatics) and Visio software (version 2013, Microsoft Corporation).  $P < 0.05$  was considered to indicate a statistically significant difference.

## Results

**High incidence of LVA-SCD occurs in early MI.** Mice with successful CAL displayed T wave elevation, verifying induction of MI. Wild-type mice subjected to MI without MitoTEMPO treatment or S2814A mutation had a high incidence ( $\sim 33.9\%$ ) of LVA-SCD within 30 min post-MI. SCD mice displayed notable T wave variation and prolonged QT, which culminated in lethal ventricular bradycardia. The surviving mice also showed prolonged QT but to a lesser extent (Fig. 1B). MitoTEMPO treatment prevented the ECG

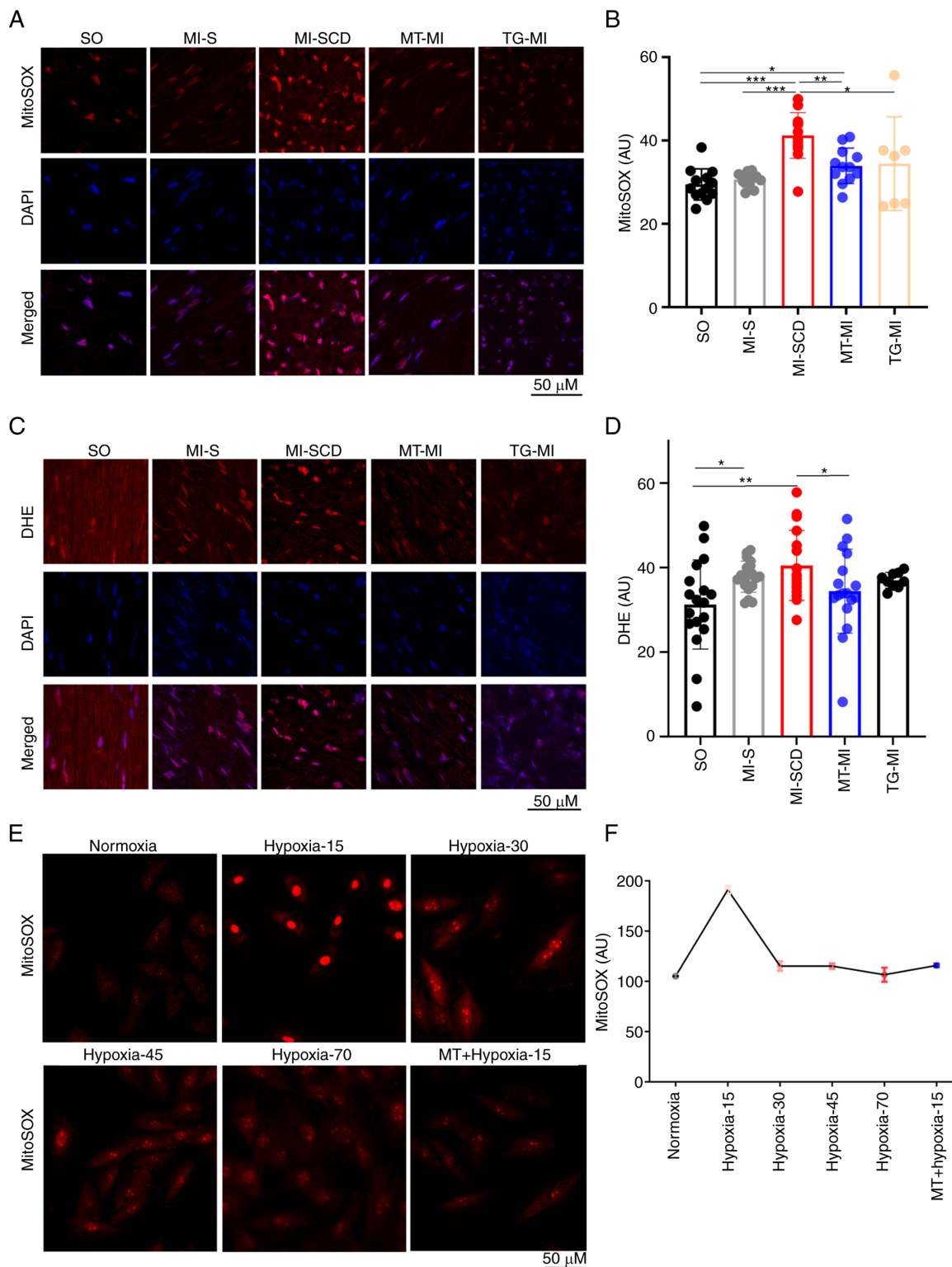


Figure 2. Early burst of mitochondrial reactive oxygen species occurs post-myocardial infarction or hypoxia. A) Representative images of MitoSOX in frozen heart sections; (B) MitoSOX intensity in different groups; (C) Representative images of DHE in frozen heart sections; (D) DHE intensity in different groups. Data were obtained from 7-20 fluorescence images from three hearts in each group. (E) Representative images displaying dynamic changes in MitoSOX intensity in H9c2 cells post-hypoxia. (F) MitoSOX intensity at each time point post-hypoxia. \*P<0.05, \*\*P<0.01, \*\*\*P<0.001. SCD, sudden cardiac death; MI, myocardial ischemia; SO, sham operation; MT, MitoTEMPO; TG, transgenic; AU, arbitrary unit.

phenotype relevant to LVA and decreased SCD incidence (14.8%). S2814A mutation was successfully constructed in C57/BL6 mice and confirmed by DNA sequencing (Fig. S1). Mutation reduced SCD incidence as well (15.6%; Fig. 1; Table SI).

*mROS burst serves a key role in the development of LVA-SCD.* LVA-SCD mice exhibited a notable increase in myocardial mROS, producing more mROS than those undergoing longer ischemia (Fig. 2A and B), suggestive of an early burst of mROS following ischemia. To validate this burst, mROS levels

were measured in H9c2 cells subjected to hypoxia (1% O<sub>2</sub>); hypoxia triggered mROS burst at ~15 min post-hypoxia; this was suppressed by MitoTEMPO (Fig. 2E and F). Therefore, the time of the high SCD incidence overlapped with the peak mROS emission after MI.

Consistently, SCD mice also demonstrated higher levels of cytosolic ROS (cytoROS), as reflected by DHE intensity (Fig. 2C and D). These mice had elevated CaMKII-M282 oxidation and RyR2-S2814 phosphorylation (Figs. 3A-C and S2; Tables SII and SIII), overloads of cytoCa<sup>2+</sup> and mitochondrial Ca<sup>2+</sup> (mitoCa<sup>2+</sup>) and lower MMP and GSH/GSSG ratio in the myocardium (Fig. 3D-I). Consistent with *in vivo* mROS results, these changes were greater in SCD mice than mice survived after MI, indicating that the SCD-induced alterations occurred in a short time.

*MitoTEMPO and S2814A mutation decrease the incidence of LVA-SCD in early MI.* Following pretreatment with MitoTEMPO, most mice survived 30 min post-MI (85.2%; Fig. 1A). MitoTEMPO inhibited the mROS burst and controlled the cytoROS production (Fig. 2C and D). As a consequence, MitoTEMPO reduced CaMKII-M282 oxidation and subsequently decreased RyR2-S2814 phosphorylation (Figs. 3A-C and S2; Tables SII and SIII), preventing overloads of myocardial cytoCa<sup>2+</sup> and mitoCa<sup>2+</sup> (Fig. 3D-G). Moreover, MitoTEMPO restored MMP, GSH/GSSG ratio and ECG alterations such as prolonged QTc and T wave variation (Figs. 1B-D and 3H and I). MitoTEMPO effectively suppressed mROS emission, mitigated Ca<sup>2+</sup> imbalance and suppressed LVA-SCD in early MI.

Similarly, most S2814A mice also survived early MI (84.4%; Fig. 1A), implying that they were protected against LVA-SCD. Of note, S2814A mutation prevented RyR2-S2814 phosphorylation despite upregulation of its upstream kinase ox-CaMKII in early MI (Fig. 3A-C). As a result, the mutation alleviated Ca<sup>2+</sup> overload both in the cytoplasm and mitochondria (Fig. 3D-G). Subsequently, S2814A mutation decreased mROS release and CaMKII-M282 oxidation (Figs. 2A-D and 3A-C). As seen with MitoTEMPO treatment, S2814A mutation partly ameliorated mitochondrial function and restored antioxidative capacity (Figs. 1D and 3H and I). These data revealed that S2814A mutation effectively corrected Ca<sup>2+</sup> imbalance, which decreased mROS production, thereby inhibiting LVA-SCD.

*Myocardial phosphoproteome remodeling in SCD is prevented by MitoTEMPO and S2814A mutation.* Changes in the myocardial phosphoproteome were assessed; 4,108 phosphorylated peptides were identified in 1,028 proteins. Phosphorylation of 583 proteins was significantly changed in SCD mice; among these, phosphorylation was up- and down-regulated in 175 and 408 proteins, respectively, compared with the SO controls. MI-S, MT-MI, and TG-MI groups exhibited fewer changes than SCD mice (Fig. 4B; Table SIV and V).

KEGG enrichment analysis of hyperphosphorylated proteins in LVA-SCD revealed enrichment in 'HIF-1 signaling pathway', citrate cycle (TCA cycle), 'Oxidative phosphorylation', 'Calcium signaling pathway', 'cGMP-PKG signaling pathway' and 'Glycolysis/gluconeogenesis' (Fig. 4C; Table SVI). Similarly, BPs were primarily enriched in

'mitochondrial ATP synthesis coupled proton transport', 'canonical glycolysis', 'NADH metabolic process', and mitochondrial electron transport', 'ubiquinol to cytochrome c' (Table SVII). Consistently, CCs were primarily enriched in the mitochondria (Fig. 4D; Table SVIII). These results suggested that hyperphosphorylation changes primarily occurred in the mitochondria. MitoTEMPO and S2814A prevented most hyperphosphorylation (Tables SIV and SV), implying that changes in the mitochondrial phosphoproteome are primarily mROS- and Ca<sup>2+</sup>-dependent and may be a key influence on the formation of the mROS-Ca<sup>2+</sup> loop.

Enrichment analysis of hypophosphorylated proteins revealed enrichment of signaling pathways, which primarily included 'insulin signaling pathway', 'spliceosome', 'AMPK signaling pathway', 'FoxO signaling pathway', 'tight junction', 'protein processing in endoplasmic reticulum', 'adipocytokine signaling pathway' and 'mTOR signaling pathway' (Fig. 4C; Tables SIX and SX). CCs were mainly enriched in the cytoplasm, different from those of hyperphosphorylated proteins (Fig. 4D; Table SXI).

## Discussion

The most important finding of the present study was the high incidence of LVA-SCD in early MI. Since mice that had a massive hemorrhage, respiratory failure and anesthesia allergy were excluded, deaths occurring in the early MI resulted from lethal bradycardia (SCD). From the electrophysiological perspective, the SCD mice were characterized by lethal bradycardia and increased T wave variation, which is associated with increased likelihood of lethal arrhythmias and SCD (23). Collectively, the present study confirmed that the early period of MI was the most common period for LVA-SCD, similar to a previous study (4).

The present study used hypoxic H9c2 cells to mimic ischemia. H9c2 cells are rat embryonic cardiomyocytes that share many features with primary mouse cardiomyocytes, especially in terms of energy metabolism patterns (such as cellular ATP levels, bioenergetics and mitochondrial function). H9c2 cells are more sensitive to hypoxic injury (24). Thus, using H9c2 cells were used to confirm hypoxia-related mROS dynamic changes. In response to hypoxia, H9c2 cells experienced an early mROS burst. Such an mROS burst has been previously demonstrated (25). Hypoxia leads to mitochondrial electron transfer chain (ETC) dysfunction, with the release of a large amount of superoxide (O<sub>2</sub><sup>•-</sup>) from complexes III and I in the ETC (26). This accumulation sensitizes the mitochondrial inner membrane anion channel (IMAC), promoting release of O<sub>2</sub><sup>•-</sup> into the cytoplasm in the form of hydrogen peroxide (27). This accounts for elevated cytoROS levels in SCD mice. Higher cytoROS levels further activate the IMAC in adjacent mitochondria, which leads to ROS-induced ROS release (RIRR) in mitochondria (28), resulting in mROS burst. Consistently, the SCD mice also demonstrated poor antioxidative capacity and mitochondrial dysfunction, as reflected by lowered GSH/GSSG ratio and MMP, both of which may facilitate the mROS burst (29,30). Another explanation for the mROS burst is that the compensatory mechanism, such as increasing expression of antioxidant proteins, has not been set up to cope with extensive oxidative stress upon early MI,

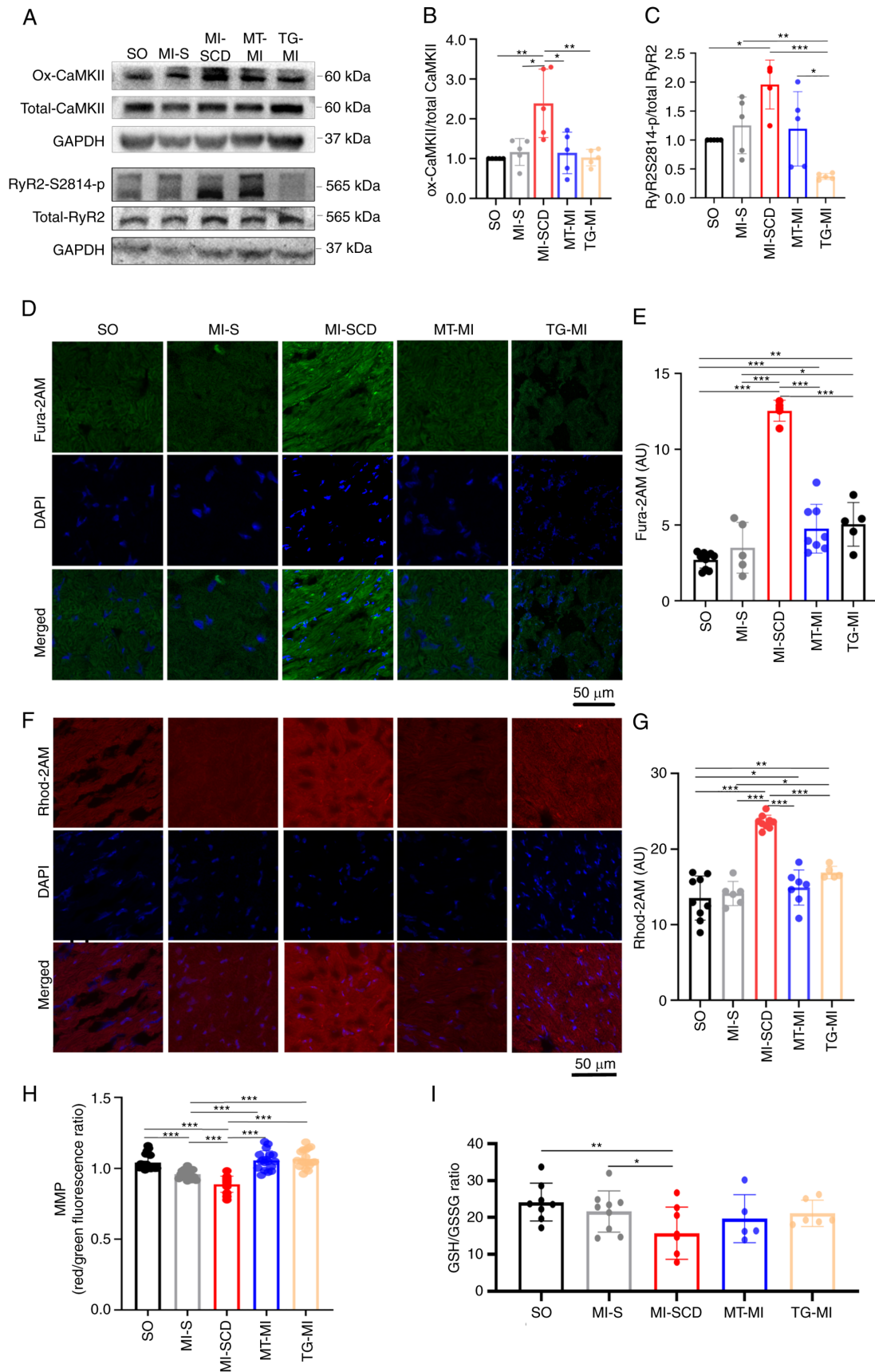


Figure 3. Increased CaMKII-M282 oxidation and RyR2-S2814 phosphorylation cause cytoCa<sup>2+</sup> and mitoCa<sup>2+</sup> overload in SCD mice. (A) Representative western blot; (B) densitometry ratio of CaMKII-M282 oxidation to total CaMKII and (C) densitometry ratio of RyR2-S2814 phosphorylation to total RyR2 (n=4-6). (D) Representative images of Fura 2-AM in frozen heart sections; (E) Fura 2-AM intensity in different groups (n=5-8). (F) Representative images of Rhod 2-AM in frozen heart sections; (G) Rhod 2-AM intensity in different groups (n=5-9); (H) MMP (14-18 fluorescence images from eight hearts in each group); (I) GSH/GSSG ratio (n=5-9). \*P<0.05, \*\*P<0.01, \*\*\*P<0.001. Ox-CaMKII, oxidized Ca<sup>2+</sup>/calmodulin-dependent protein kinase; p-RyR2-S2814, phosphorylation of ryanodine receptor 2 at Ser2814; cyto, cytoplasm; mito, mitochondria; MMP, mitochondrial membrane potential; GSH, reduced glutathione; GSSG, oxidized glutathione; SCD, sudden cardiac death; MI, myocardial ischemia; SO, sham operation; MT, MitoTEMPO; TG, transgenic; AU, arbitrary unit.

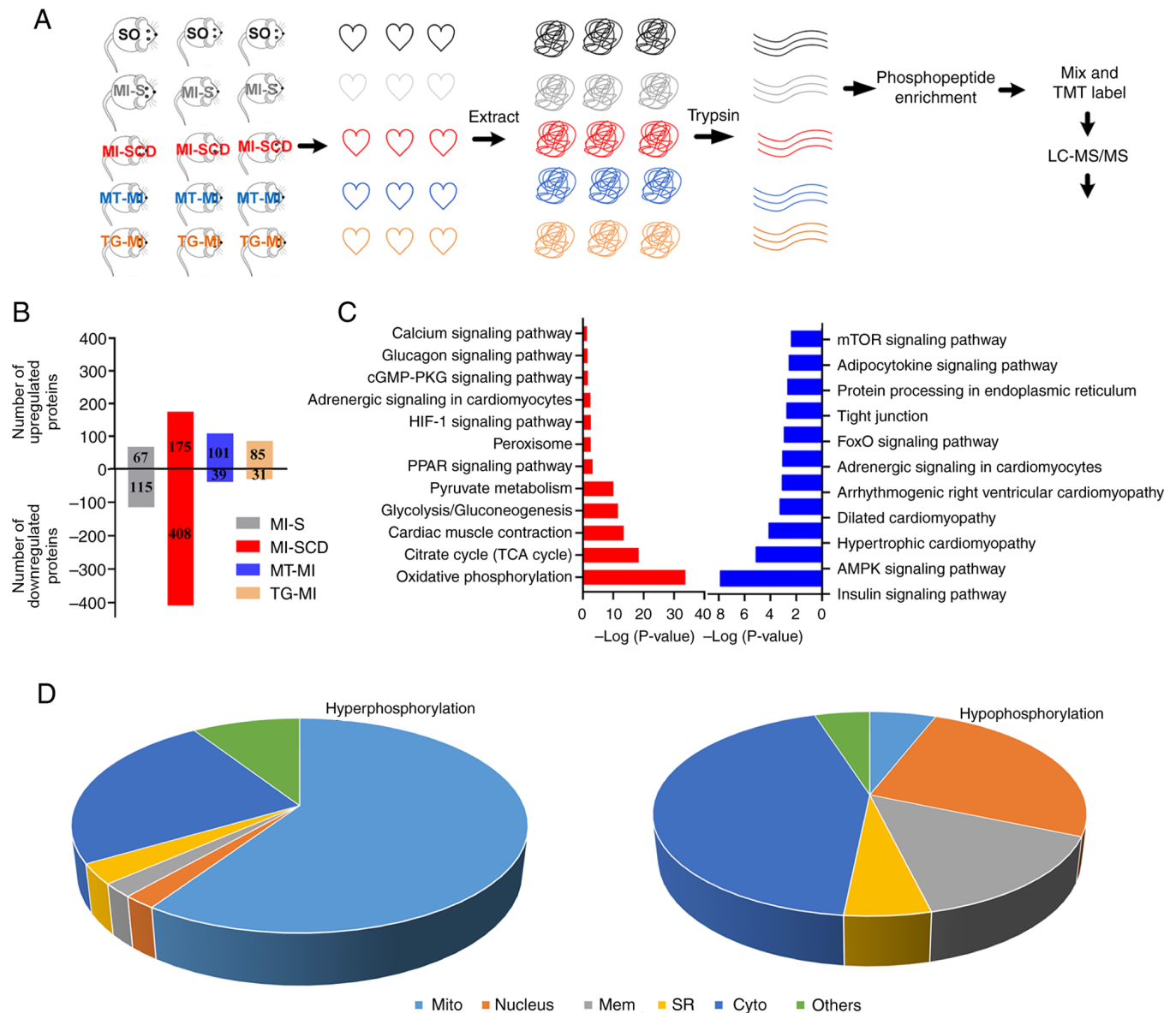


Figure 4. Myocardial phosphoproteome alterations in SCD and surviving mice. (A) Design of phosphoproteome experiments. (B) SCD mice exhibited more alterations in protein phosphorylation than the surviving mice. (C) Representative enriched Kyoto Encyclopedia of Genes and Genomes pathways in the SCD mice. Red, upregulation; blue, downregulation. (D) Cellular components of hyperphosphorylated proteins in SCD mice were primarily enriched in the mitochondria, whereas those of hypophosphorylated proteins were primarily enriched in the cytoplasm. SCD, sudden cardiac death; SO, sham operation; MI, myocardial ischemia; S, stable; MT, MitoTEMPO; TG, transgenic; TMT, Tandem Mass Tag; LC-MS, Liquid Chromatography-Mass Spectrometry; mito, mitochondria; mem, membrane; SR, sarcoplasmic reticulum; cyto, cytoplasm.

hence allowing RIRR (31). However, with increased duration of ischemia, myocytes establish a compensatory mechanism to reduce excessive mROS (32), as indicated by lowered GSH/GSSG ratio and restoration of MMP almost to normal levels in surviving mice.

Expectedly, MitoTEMPO, a combination of the antioxidant TEMPO (2,2,6,6-tetramethylpiperidinyl-1-oxyl) and lipophilic cation triphenyl phosphonium that is capable of targeted removal of mROS (33), corrected SCD-associated alterations induced by mROS, demonstrating the effects of mROS burst on LVA-SCD development. Therefore, the effect of mROS- $Ca^{2+}$  interaction in LVA-SCD was assessed using S2814A mice. Apart from the expected findings that the transgenic mice exhibited decreased RyR2(Ser2814) phosphorylation and  $Ca^{2+}$  content in the cytoplasm and mitochondria, the mutation decreased the

levels of mROS, which indicated that the early mROS burst was  $Ca^{2+}$ -dependent. Mito $Ca^{2+}$  overload activates protein kinase C (PKC) and subsequently increase mROS (34). PKC enhances phosphorylation of ETC proteins, which facilitates mROS production (35). On the other hand, excessive mROS lead to diastolic  $Ca^{2+}$  leak and  $Ca^{2+}$  overload via the mROS-oxidized CaMKII(M281)/phosphorylated RyR2(S2814) pathway. ROS directly oxidize RyR2 and cause  $Ca^{2+}$  leakage. However, under oxidative stress, increased RyR2 phosphorylation occurs earlier than RyR2 oxidation (36). Therefore, the activation of the above pathway is a primary mechanism leading to  $Ca^{2+}$  imbalance. Altogether,  $Ca^{2+}$  imbalance and mROS may form an mROS- $Ca^{2+}$  loop that promotes LVA-SCD in early MI (Fig. 5). MitoTEMPO and S2814A mutation block this loop and effectively curb LVA-SCD.

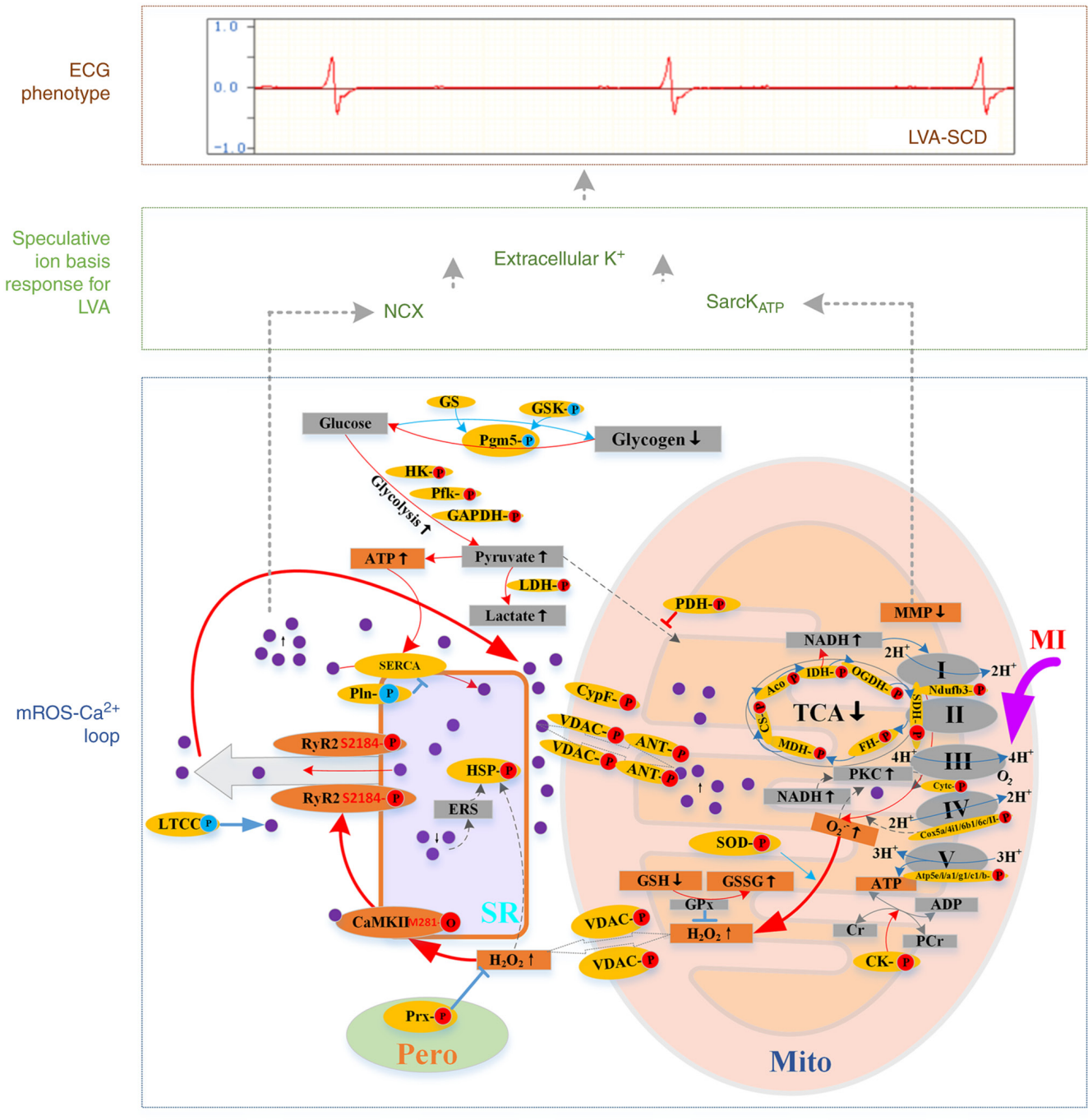


Figure 5. Scheme depicting the crosstalk of mROS/ROS and Ca<sup>2+</sup> signaling pathways and proposed relevant ion bases that promote LVA-SCD. Red, upregulation; blue, downregulation; purple circle, calcium ion. Mito, mitochondria; SR, sarcoplasmic reticulum; I-V, Complex I-V; Cyt c, cytochrome C; COX, cytochrome oxidase; Atp5, ATP synthase; SOD, superoxide dismutase; VDAC, voltage-dependent anion channel; Cyp F, cyclophilin F/peptidylprolyl isomerase F; ANT, adenine nucleotide translocase; MDH, malate dehydrogenase; CS, citrate synthase; IDH, isocitrate dehydrogenase; SDH, succinate dehydrogenase; OGDH, oxoglutarate dehydrogenase; FH, fumarate hydratase; ERS, endoplasmic reticulum stress; HSP, heat shock protein; HK, hexokinase; Pfk, phosphofruktokinase; PDH, pyruvate dehydrogenase; PKC, protein kinase C; SERCA, sarco/endoplasmic reticulum Ca<sup>2+</sup> ATPase; Pln, phospholamban; LTCC, L-type calcium channel; NCX, Na<sup>+</sup>/Ca<sup>2+</sup> exchanger; sarcK<sub>ATP</sub>, sarcolemmal ATP-sensitive K<sup>+</sup> channel; ECG, electrocardiogram; mROS, mitochondrial ROS; MI, myocardial ischemia; TCA, tricarboxylic acid; Aco, aconitase; pero, peroxisome; Mito, mitochondria; PCr, Phosphocreatine; CK, creatine kinase; LVA-SCD, lethal ventricular arrhythmia-sudden cardia death.

Phosphorylation is a key post-translational mechanism that participates in rapid pathophysiological processes (37). Following a short period of MI, the SCD mice exhibited notable phosphoproteome changes. Surviving mice that experienced longer ischemia had fewer changes in phosphoprotein levels. Notably, most hyperphosphorylated proteins were localized in the mitochondria and primarily involved in redox homeostasis,

ion transport, mitochondrial electron transport and energy balance. Elevated Ca<sup>2+</sup> and ROS activate PKC, which may be responsible for hyperphosphorylation (34). ETC-localized proteins were hyperphosphorylated in SCD, which decreases ETC function, thereby promoting O<sub>2</sub> burst (38,39). Meanwhile, enzymes involved in the TCA cycle were hyperphosphorylated, which has been shown to inhibit the TCA cycle (40).

Furthermore, voltage-dependent anion channel (VDAC), peptidylprolyl isomerase F (cyclophilin F) and adenine nucleotide translocase A4/5 (ANT) were hyperphosphorylated in LVA-SCD. VDAC hyperphosphorylation favors its closure, increasing  $\text{Ca}^{2+}$  influx into mitochondria (41). Phosphorylation of cyclophilin F and ANT facilitate mPTP opening (41,42). These findings explain Mito $\text{Ca}^{2+}$  concomitant with cyto $\text{Ca}^{2+}$  overload in mice that underwent SCD. In addition, superoxide mutase (SOD) was hyperphosphorylated, which inactivates its function, thereby allowing local  $\text{O}_2^-$  accumulation (43). Therefore, hyperphosphorylation of mitochondrial protein was mainly related to the aggravation of mitochondrial dysfunction and subsequent induction of the mROS/ $\text{Ca}^{2+}$  cycle. Additionally glycolysis-associated enzymes were hyperphosphorylated in LVA-SCD, which may activate these enzymes and enhance glycolysis (44,45). SCD mice exhibited higher levels of mROS as well as significant mitochondrial protein phosphorylation alteration; these phosphorylation alterations were prevented by MitoTEMPO, and S2814A mutation, which decreased mROS levels in MI mice, could also normalize the phosphorylated disturbance; therefore, it was hypothesized that most mitochondria-associated phosphorylated alterations were associated with the mROS/ $\text{Ca}^{2+}$  loop.

Upon formation of the mROS/ $\text{Ca}^{2+}$  loop, several factors contribute to the occurrence of lethal ventricular bradycardia. First, excessive mROS cause mitochondrial metabolic sink, a state that cardiomyocytes are rendered inexcitable because of the large background  $\text{K}^+$  (46). Second, cytoplasmic  $\text{Ca}^{2+}$  overload leads to cytoplasmic  $\text{Na}^+$  overload by activating the  $\text{Na}^+/\text{Ca}^{2+}$  exchanger, which further facilitates net intracellular net  $\text{K}^+$  loss because of the need to maintain electroneutrality and osmotic balance (47). Additionally, enhanced glycolysis increases intracellular  $\text{H}^+$ , which activates  $\text{Na}^+/\text{H}^+$  exchanger (48). All these alterations result in extracellular  $\text{K}^+$  accumulation and decrease electrical conduction within the ventricle, as displayed in ECG in LVA-SCD.

A limitation of the present study is that  $\text{Ca}^{2+}$  concentration was not detected dynamically. Here, frozen sections were made immediately after death when notable cell membrane damage did not occur. Meanwhile, some free  $\text{Ca}^{2+}$  may be released to the extracellular compartment during slice preparation, which may cause signals from extracellular areas. Since contraction requires excitation, the myocardium was maintained in diastole after death because the excitation stopped. Therefore, myocardial  $\text{Ca}^{2+}$  content represents  $\text{Ca}^{2+}$  content in diastole.

In conclusion, early post-MI is the most common stage for SCD. The formation of an mROS/ $\text{Ca}^{2+}$  loop plays a critical role in promoting LVA-SCD. Mitochondrial proteomic hyperphosphorylation may facilitate formation of this loop. Both MitoTEMPO treatment and S2814A mutation prevent SCD-associated changes and LVA-SCD. The present data imply an association between mROS and  $\text{Ca}^{2+}$  imbalance, which warns that we need to prevent the formation of the mROS/ $\text{Ca}^{2+}$  loop to effectively control early SCD post-MI.

### Acknowledgements

The authors would like to thank Dr Ricardo Carnicer Hijazo (University of Oxford, Oxford, UK) and Professor Stanley Lin (SUMC, Shantou, China) for editing the manuscript.

### Funding

The present study was supported by the Guangdong Province General University Characteristic Innovation Project (grant no. 2021KTSCX032), Guangdong Natural Science Foundation (grant no. 2022A1515011119) and Innovative Team Research Program for Universities of Guangdong Province (grant no. 2022KCXTD009).

### Availability of data and materials

The datasets used and/or analyzed during the current study are available from the corresponding author upon reasonable request.

### Authors' contributions

DZ, YeZ, MZhu, XiaojuaZ, XiaojunZ, WT, QW, YL, LT, ZZ, JL, YaZ and DW performed the experiments. DW designed the study. DW and DZ wrote the manuscript. DZ, YeZ, MZhu, ML, DW and MZha analyzed the data. All authors have read and approved the final manuscript. DW and DZ confirm the authenticity of all the raw data.

### Ethics approval and consent to participate

The study was approved by the Medical Animal Care and Welfare Committee at Shantou University Medical College (approval no. SUMC2020-035).

### Patient consent for publication

Not applicable.

### Competing interests

The authors declare that they have no competing interests.

### References

1. World Health Organization (WHO): The top 10 causes of death. WHO, Geneva, 2020. <https://www.who.int/news-room/fact-sheets/detail/the-top-10-causes-of-death>.
2. Chugh SS, Reinier K, Teodorescu C, Evanado A, Kehr E, Al Samara M, Mariani R, Gunson K and Jui J: Epidemiology of sudden cardiac death: Clinical and research implications. *Prog Cardiovasc Dis* 51: 213-228, 2008.
3. Al-Khatib SM, Stevenson WG, Ackerman MJ, Bryant WJ, Callans DJ, Curtis AB, Deal BJ, Dickfeld T, Field ME, Fonarow GC, *et al*: 2017 AHA/ACC/HRS Guideline for Management of Patients With Ventricular Arrhythmias and the Prevention of Sudden Cardiac Death: Executive Summary: A Report of the American College of Cardiology/American Heart Association Task Force on Clinical Practice Guidelines and the Heart Rhythm Society. *Circulation* 138: e210-e271, 2018.
4. Zaman S and Kovoor P: Sudden cardiac death early after myocardial infarction: Pathogenesis, risk stratification, and primary prevention. *Circulation* 129: 2426-2435, 2014.
5. Reed GW, Rossi JE and Cannon CP: Acute myocardial infarction. *Lancet* 389: 197-210, 2017.
6. Jeong EM, Liu M, Sturdy M, Gao G, Varghese ST, Sovari AA and Dudley SC Jr: Metabolic stress, reactive oxygen species, and arrhythmia. *J Mol Cell Cardiol* 52: 454-463, 2012.
7. Csordas G, Weaver D and Hajnoczky G: Endoplasmic Reticulum-Mitochondrial Contactology: Structure and signaling functions. *Trends Cell Biol* 28: 523-540, 2018.

8. Wang JJ, Park KS, Dhimal N, Shen S, Tang X, Qu J and Zhang SX: Proteomic analysis of retinal mitochondria-associated ER membranes identified novel proteins of retinal degeneration in long-term diabetes. *Cells* 11: 2819, 2022.
9. Liu X, Wang S, Guo X, Li Y, Ogurlu R, Lu F, Prondzynski M, de la Serna Buzon S, Ma Q, Zhang D, *et al*: Increased Reactive Oxygen Species-Mediated Ca(2+)/calmodulin-dependent protein kinase II activation contributes to calcium handling abnormalities and impaired contraction in Barth syndrome. *Circulation* 143: 1894-1911, 2021.
10. Bertero E and Maack C: Calcium signaling and reactive oxygen species in mitochondria. *Circ Res* 122: 1460-1478, 2018.
11. Purohit A, Rokita AG, Guan X, Chen B, Koval OM, Voigt N, Neef S, Sowa T, Gao Z, Luczak ED, *et al*: Oxidized Ca(2+)/calmodulin-dependent protein kinase II triggers atrial fibrillation. *Circulation* 128: 1748-1757, 2013.
12. van Oort RJ, McCauley MD, Dixit SS, Pereira L, Yang Y, Respress JL, Wang Q, De Almeida AC, Skapura DG, Anderson ME, *et al*: Ryanodine receptor phosphorylation by calcium/calmodulin-dependent protein kinase II promotes life-threatening ventricular arrhythmias in mice with heart failure. *Circulation* 122: 2669-2679, 2010.
13. National Research Council of The National Academies: Guide for the Care and Use of Laboratory Animals. 8th Edition. National Academy Press, Washington, DC, 2011.
14. Albert CM, McGovern BA, Newell JB and Ruskin JN: Sex differences in cardiac arrest survivors. *Circulation* 93: 1170-1176, 1996.
15. Jasmin M, Ahn EH, Voutilainen MH, Fombonne J, Guix C, Viljakainen T, Kang SS, Yu LY, Saarna M, Mehlen P and Ye K: Netrin-1 and its receptor DCC modulate survival and death of dopamine neurons and Parkinson's disease features. *EMBO J* 40: e105537, 2021.
16. Koshy AN, Gow PJ, Testro A, Th AW, Ko J, Lim HS, Han HC, Weinberg L, VanWagner LB and Farouque O: Relationship between QT interval prolongation and structural abnormalities in cirrhotic cardiomyopathy: A change in the current paradigm. *Am J Transplant* 21: 2240-2245, 2021.
17. Dey S, DeMazumder D, Sidor A, Foster DB and O'Rourke B: Mitochondrial ROS drive sudden cardiac death and chronic proteome remodeling in heart failure. *Circ Res* 123: 356-371, 2018.
18. Xie D, Wu J, Wu Q, Zhang X, Zhou D, Dai W, Zhu M and Wang D: Integrating proteomic, lipidomic and metabolomic data to construct a global metabolic network of lethal ventricular tachyarrhythmias (LVTa) induced by aconitine. *J Proteomics* 232: 104043, 2021.
19. Friedrich C, Schallenberg S, Kirchner M, Ziehm M, Niquet S, Haji M, Beier C, Neudecker J, Klauschen F and Mertins P: Comprehensive micro-scaled proteome and phosphoproteome characterization of archived retrospective cancer repositories. *Nat Commun* 12: 3576, 2021.
20. Cox J and Mann M: MaxQuant enables high peptide identification rates, individualized p.p.b.-range mass accuracies and proteome-wide protein quantification. *Nat Biotechnol* 26: 1367-1372, 2008.
21. Choi M, Chang CY, Clough T, Broudy D, Killeen T, MacLean B and Vitek O: MSstats: An R package for statistical analysis of quantitative mass spectrometry-based proteomic experiments. *Bioinformatics* 30: 2524-2526, 2014.
22. Shang L, Wang Y, Li J, Zhou F, Xiao K, Liu Y, Zhang M, Wang S and Yang S: Mechanism of Sijunzi Decoction in the treatment of colorectal cancer based on network pharmacology and experimental validation. *J Ethnopharmacol* 302(Pt A): 115876, 2023.
23. Ramirez J, Orini M, Minchola A, Monasterio V, Cygankiewicz I, Bayés de Luna A, Martínez JP, Pueyo E and Laguna P: T-Wave morphology restitution predicts sudden cardiac death in patients with chronic heart failure. *J Am Heart Assoc* 6: e005310, 2017.
24. Kuznetsov AV, Javadov S, Sickinger S, Frotschnig S and Grimm M: H9c2 and HL-1 cells demonstrate distinct features of energy metabolism, mitochondrial function and sensitivity to hypoxia-reoxygenation. *Biochim Biophys Acta* 1853: 276-284, 2015.
25. Hernansanz-Agustin P, Choya-Foces C, Carregal-Romero S, Ramos E, Oliva T, Villa-Piña T, Moreno L, Izquierdo-Álvarez A, Cabrera-García JD, Cortés A, *et al*: Na(+) controls hypoxic signalling by the mitochondrial respiratory chain. *Nature* 586: 287-291, 2020.
26. Yang KC, Kyle JW, Makielski JC and Dudley SC Jr: Mechanisms of sudden cardiac death: Oxidants and metabolism. *Circ Res* 116: 1937-1955, 2015.
27. Akar FG, Aon MA, Tomaselli GF and O'Rourke B: The mitochondrial origin of posts ischemic arrhythmias. *J Clin Invest* 115: 3527-3535, 2005.
28. Zorov DB, Juhaszova M and Sollott SJ: Mitochondrial reactive oxygen species (ROS) and ROS-induced ROS release. *Physiol Rev* 94: 909-950, 2014.
29. Schafer FQ and Buettner GR: Redox environment of the cell as viewed through the redox state of the glutathione disulfide/glutathione couple. *Free Radic Biol Med* 30: 1191-1212, 2001.
30. Bagkos G, Koufopoulos K and Piperi C: A new model for mitochondrial membrane potential production and storage. *Med Hypotheses* 83: 175-181, 2014.
31. Crewe C, Funcke JB, Li S, Joffin N, Gliniak CM, Ghaben AL, An YA, Sadek HA, Gordillo R, Akgul Y, *et al*: Extracellular vesicle-based interorgan transport of mitochondria from energetically stressed adipocytes. *Cell Metab* 33: 1853-1868 e11, 2021.
32. Ferko M, Andelova N, Szeiffova Bacova B and Jasova M: Myocardial adaptation in pseudohypoxia: Signaling and Regulation of mPTP via mitochondrial connexin 43 and cardiolipin. *Cells* 8: 1449, 2019.
33. Shetty S, Kumar R and Bharati S: Mito-TEMPO, a mitochondria-targeted antioxidant, prevents N-nitrosodiethylamine-induced hepatocarcinogenesis in mice. *Free Radic Biol Med* 136: 76-86, 2019.
34. Hegyi B, Borst JM, Bailey LRJ, Shen EY, Lucena AJ, Navedo MF, Bossuyt J and Bers DM: Hyperglycemia regulates cardiac K(+) channels via O-GlcNAc-CaMKII and NOX2-ROS-PKC pathways. *Basic Res Cardiol* 115: 71, 2020.
35. Rebollo-Hernanz M, Zhang Q, Aguilera Y, Martin-Cabrejas MA and Gonzalez de Mejia E: Relationship of the phytochemicals from coffee and cocoa by-products with their potential to modulate biomarkers of metabolic syndrome in vitro. *Antioxidants (Basel)* 8: 279, 2019.
36. Belevych AE, Terentyev D, Terentyeva R, Nishijima Y, Sridhar A, Hamlin RL, Carnes CA and Györke S: The relationship between arrhythmogenesis and impaired contractility in heart failure: Role of altered ryanodine receptor function. *Cardiovasc Res* 90: 493-502, 2011.
37. Humphrey SJ, James DE and Mann M: Protein Phosphorylation: A major switch mechanism for metabolic regulation. *Trends Endocrinol Metab* 26: 676-687, 2015.
38. Kalpage HA, Wan J, Morse PT, Zurek MP, Turner AA, Khobeir A, Yazdi N, Hakim L, Liu J, Vaishnav A, *et al*: Cytochrome c phosphorylation: Control of mitochondrial electron transport chain flux and apoptosis. *Int J Biochem Cell Biol* 121: 105704, 2020.
39. Kane LA, Youngman MJ, Jensen RE and Van Eyk JE: Phosphorylation of the F(1)F(o) ATP synthase beta subunit: Functional and structural consequences assessed in a model system. *Circ Res* 106: 504-513, 2010.
40. Guo X, Niemi NM, Hutchins PD, Condon SGF, Jochem A, Ulbrich A, Higbee AJ, Russell JD, Senes A, Coon JJ and Pagliarini DJ: Ptc7p dephosphorylates select mitochondrial proteins to enhance metabolic function. *Cell Rep* 18: 307-313, 2017.
41. Wang Z, Ge Y, Bao H, Dworkin L, Peng A and Gong R: Redox-sensitive glycogen synthase kinase 3β-directed control of mitochondrial permeability transition: Rheostatic regulation of acute kidney injury. *Free Radic Biol Med* 65: 849-858, 2013.
42. Feng J, Zhu M, Schaub MC, Gehrig P, Roschitzki B, Lucchinetti E and Zaugg M: Phosphoproteome analysis of isoflurane-protected heart mitochondria: Phosphorylation of adenine nucleotide translocator-1 on Tyr194 regulates mitochondrial function. *Cardiovasc Res* 80: 20-29, 2008.
43. Banks CJ and Andersen JL: Mechanisms of SOD1 regulation by post-translational modifications. *Redox Biol* 26: 101270, 2019.
44. Dieni CA and Storey KB: Regulation of hexokinase by reversible phosphorylation in skeletal muscle of a freeze-tolerant frog. *Comp Biochem Physiol B Biochem Mol Biol* 159: 236-243, 2011.
45. Lee JH, Liu R, Li J, Wang Y, Tan L, Li XJ, Qian X, Zhang C, Xia Y, Xu D, *et al*: EGFR-Phosphorylated platelet isoform of phosphofructokinase 1 promotes PI3K activation. *Mol Cell* 70: 197-210 e7, 2018.
46. Akar FG and O'Rourke B: Mitochondria are sources of metabolic sink and arrhythmias. *Pharmacol Ther* 131: 287-294, 2011.
47. Landstrom AP, Dobrev D and Wehrens XHT: Calcium signaling and cardiac arrhythmias. *Circ Res* 120: 1969-1993, 2017.
48. Barth AS and Tomaselli GF: Cardiac metabolism and arrhythmias. *Circ Arrhythm Electrophysiol* 2: 327-335, 2009.

